Analytical Methods

ROYAL SOCIETY OF CHEMISTRY

TECHNICAL NOTE

View Article Online
View Journal | View Issue

Cite this: *Anal. Methods*, 2026, **18**, 1541

Optimization of aptamer-triggered hybridization chain reaction for rapid visual ATP detection using gold nanoparticles

Shengli Zhou, [a] Hiroko Fukaya,[a] Shunsuke Watanuki,[a] Wei Liu, [a] Maasa Yokomori, [a] Muneyuki Matsuo, [ac] Kazuya Okada,[b] Yukina Yoshioka[b] and Keitaro Yoshimoto *[a]

The development of fast, simple, and visual methods for detecting adenosine triphosphate (ATP) is crucial for point-of-care diagnostics and environmental monitoring. Colorimetric assays based on the integration of DNA aptamer-triggered hybridization chain reaction (HCR) with gold nanoparticles (AuNPs) offer high potential, but existing methods often suffer from prolonged detection times (*e.g.*, >130 min). To address this limitation, this study systematically investigated and optimized the core parameters of the aptamer-triggered HCR system and its subsequent mixing conditions with AuNPs to achieve a rapid visual detection platform. The HCR kinetics were accelerated by the high concentrations of single-stranded DNA (ssDNA) components, particularly the H0 initiator, as well as by the critical presence of divalent magnesium ions (Mg^{2+}), which also support the functionality of the aptamer. This optimization allowed for a degree of HCR progression comparable to the traditional 24-hour incubation to be achieved within just 60 minutes. Subsequently, recognizing the inherent trade-off between the high ssDNA concentration required for fast HCR and the AuNP dispersion stability, we optimized the mixing ratio between the HCR product and the AuNP solution. Under these optimized conditions, the assay demonstrated the capability for rapid visual detection of ATP at the 100 μM level within a total assay time of 15 minutes, representing a significant acceleration compared to previously reported methods. Further improvements in sensitivity are anticipated through future fine-tuning of AuNP parameters and the use of post-reaction salt aggregation enhancers.

Received 17th October 2025
Accepted 2nd February 2026

DOI: 10.1039/d5ay01738f

rsc.li/methods

Introduction

Adenosine triphosphate (ATP), a central molecule in cellular energy metabolism, serves as a critical biomarker for assessing microbial contamination and hygiene status across diverse industries, including food production, pharmaceuticals, and cosmetics.[1–5] Conventional ATP detection predominantly relies on luciferase-catalyzed bioluminescent reactions, implemented in portable ATP fluorescence detectors widely deployed in industrial settings.[6,7] While offering rapid response and operational simplicity, these methods remain heavily dependent on dedicated instrumentation.[6–8] This reliance introduces significant limitations for resource-constrained environments or challenging field conditions, stemming from their need for power sources, sensitivity to ambient light, and susceptibility to operator-dependent variability.

In recent years, colorimetric detection platforms integrating DNA aptamers with gold nanoparticles (AuNPs) have emerged as promising alternatives, offering instrument-free operation and visually interpretable results.[9–16] For instance, Yang *et al.* developed an aptamer–AuNP sensor for ochratoxin A detection with a limit of detection (LOD) of 20 nM using UV-vis spectrophotometer.[14] Similarly, Tu *et al.* reported a conjugated aptamer–AuNP probe for amyloid-β oligomers achieving an LOD of 3.03 nM, highlighting its diagnostic potential also using UV-vis spectrophotometer.[15] Zhu *et al.* further demonstrated excellent sensitivity (LOD = 26 cells per mL) using potentiostat/galvanostat with a hydrazine–AuNP–aptamer bioconjugate for specific breast cancer cell recognition.[16]

The color change of AuNPs is useful for developing the visual detection method. To enhance the sensitivity of visual detection, aptamer-triggered hybridization chain reaction (HCR), an enzyme-free isothermal amplification mechanism, has been frequently integrated with AuNP-based colorimetric systems.[17–24] However, existing HCR–AuNP platforms still face practical limitations in terms of reaction time. For example,

[a]*Department of Life Sciences, Graduate School of Arts and Sciences, The University of Tokyo, 3-8-1 Komaba, Meguro, Tokyo, 153-8902, Japan. E-mail: ckeitaro@mail.ecc.u-tokyo.ac.jp*

[b]*Daikin Industries, Ltd, 1-1 Nishi-Hitotsuya, Settsu-shi, Osaka, 566-8585, Japan*

[c]*Graduate School of Integrated Science for Life, Hiroshima University, 1-3-1 Kagamiyama, Higashi-Hiroshima, Hiroshima, 739-8526, Japan*

Dirks *et al.* first reported the aptamer-triggered HCR using three single-stranded DNAs (ssDNAs) and required an extremely long reaction time of up to 24 hours to confirm HCR products *via* gel electrophoresis. Then, Gao *et al.* proposed a visual ATP detection method based on a mixture of HCR products and AuNPs, in which they used two ssDNAs for HCR and AuNPs synthesized by themselves. ATP could be detected with a reported LOD of 1.0 nM, which was evaluated based on UV-vis spectroscopic analysis of the absorbance ratio (A_{630}/A_{520}).[25] Although Gao *et al.* developed a visual ATP detection assay by mixing the HCR products with AuNPs, their procedure still required approximately 130 minutes with 37 °C.

Such lengthy, instrument-dependent and heating required workflows significantly hinder their feasibility for rapid on-site testing applications. Therefore, the primary objective of this study was to optimize the procedure by refine the experimental conditions of the essential components constituting this aptamer-triggered HCR-based detection system. Specifically, we focused on the total ssDNA concentration, NaCl concentration, and $MgCl_2$ concentration. Finally, we demonstrated the visual ATP detection within 15 minutes with 25 °C.

Results and discussion

Experimental system design

In evaluating and optimizing this experimental system, we employed three ssDNA strands for the aptamer-triggered HCR, originally designed by Dirks *et al.*, using commercially available AuNPs. Fig. 1 shows the illustration of the outline for the ATP visual detection method investigated in this study, which is based on the ATP-binding DNA aptamer-triggered HCR with AuNPs. In the absence of ATP, the H0 strand maintains a stable stem-loop conformation, preventing unintended initiation of HCR. Upon the introduction of ATP, the ATP-specific aptamer segment located at the 3′-end of H0 rapidly binds to the target molecule, triggering a conformational switch. This exposes the initiator sequence at the 5′-end of H0, which subsequently hybridizes with H1. The conformational change of H1 then facilitates its hybridization with H2, thereby initiating a cascade of alternating hybridization events between H1 and H2 that result in the formation of long, nicked double-stranded DNA polymers through HCR. After sufficient amplification, AuNPs are added to the reaction mixture. The high molecular weight HCR products are generated, which reduces the amount of free ssDNA substrates that can adsorb onto the surface of AuNPs. As a result, the AuNPs aggregation and inducing a distinct color change from red to bluish-purple due to the plasmon coupling effect. In contrast, if ATP is absent or the HCR is not efficiently initiated, only short ssDNA strands are present in solution. These low-molecular-weight DNA strands densely coat the AuNP surface, imparting strong electrostatic repulsion between AuNPs and maintaining a well-dispersed state, thus preserving the characteristic red color of AuNPs.

At first, we investigated the factors that accelerate the aptamer-triggered HCR by the gel electrophoresis analysis. Specifically, we focused on the total ssDNA concentration, NaCl concentration, and $MgCl_2$ concentration. Then, the rapid visual ATP detection using AuNPs was demonstrated.

Optimization of experimental condition for HCR

The ssDNA sequences used in this study are summarized in Table 1. Among them, H0 contains the ATP-binding DNA aptamer sequence. The DNA aptamer ACCTGGGGGAGTATTGCGGAGGAAGGT has been reported to bind adenosine, adenosine triphosphate (ATP), and adenosine monophosphate (AMP) at micromolar concentrations,[26] whose three-dimensional structure can be observed in the Protein Data Bank as a 1AW4 PDB file. Three ssDNA strands—H0 (which contains the ATP-binding DNA aptamer sequence), H1, and H2—were reacted to generate an HCR product with a high molecular weight. As the concentration of added ATP varied, the HCR reaction rate changed accordingly, resulting in a corresponding variation in the amount of unreacted H0, H1, and H2 remaining in the solution. As the HCR progressed, the quantity of H0, H1, and H2 decreased in the solution. These H0, H1, and H2 ssDNAs contain a non-complementary sequence region that

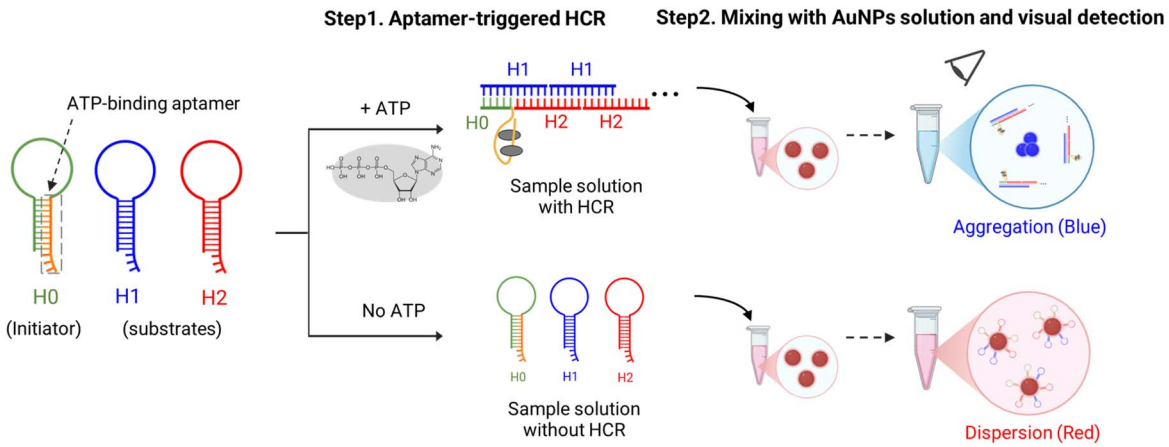

Fig. 1 Schematic illustration of the aggregation and dispersion of gold nanoparticles (AuNPs) based on an aptamer-triggered hybridization chain reaction (HCR) triggered by ATP.

Table 1 Nucleotide sequence of ssDNAs for aptamer-triggered HCR used in this study

Name	Sequences (5′ to 3′)[a]
H0 (initiator)	CCC AGG TAA CAA GAA AGC CAA ACC TCT TGT TAC CTG GGG GAG TAT TGC GGA GGA AGG T
H1 (substrate)	TAA CAA GAA AGC CAA ACC GAG ATG GGT TTG GCT TTC TTG TTA CCT GGG
H2 (substrate)	CAT CTC GGT TTG GCT TTC TTG TTA CCC AGG TAA CAA GAA AGC CAA ACC

[a] Sequence of ATP binding aptamer is represented by solid underline. Hybridization sequences are represented using double underlines or wavy underlines.

facilitates their adsorption onto the surface of AuNPs. The adsorption of these ssDNAs enhances the dispersion stability of the AuNPs in the aqueous solution, causing the solution to appear red, while, in the case of ATP addition, the total ssDNA concentration decreased, causing the solution to appear blue as shown in Fig. 1.

The total concentration of the ssDNA components is typically the most significant factor affecting the reaction rate of HCR, as it directly impacts the collision frequency of the hairpin structures (H1 and H2) and the initiator (H0). To investigate this effect, we conducted HCR reactions for 24 hours while varying the initial concentration of H0, H1, and H2 from 1 μM to 6 μM (*i.e.*, [H0] = [H1] = [H2]). The resulting HCR products were subsequently evaluated using gel electrophoresis (Fig. 2A). As shown in Fig. 2A, the ATP-containing samples exhibited distinct bands corresponding to the HCR polymerization products in the high molecular weight region. Simultaneously, a clear decrease in the band intensity of the monomer ssDNA substrates, H1 and H2, was observed. Fig. 2B shows the quantitative analysis of the H1 and H2 band intensities in Fig. 2A confirmed the expected outcome: the HCR reaction rate, quantified by the total consumption ratio of H1 and H2, increased proportionally with the increase in the total ssDNA concentration. Specifically, under the 24-hour HCR condition of [H0] = [H1] = [H2] = 1 μM, which corresponds to the concentration set by Dirks *et al.* in their previous study, a consumption ratio of approximately 44.2% was observed. By increasing the ssDNA concentration 6-fold, *i.e.*, to [H0] = [H1] = [H2] = 6 μM, the consumption ratio of H1 and H2 nearly doubled to 84.1%. Furthermore, the 4 μM condition also demonstrated a high consumption ratio of 77.8%.

To further investigate the HCR process, we performed a time-dependent analysis of the HCR reaction over a shorter period (0–120 minutes). Fig. 3A shows the total consumption of the H1 and H2 substrates over time under various equal ssDNA concentrations ([H0] = [H1] = [H2] = 2, 4, and 6 μM) with different reaction times. As anticipated, the total consumption ratio of H1 and H2 increased with both higher ssDNA concentration and longer reaction time. Notably, for the highest concentration tested (6 μM), the consumption ratio reached approximately 30% after 60 and 120 minutes of reaction time. While this demonstrated the benefit of higher concentration, the overall consumption rate within the 2-hour window remained insufficient for maximizing the signal, suggesting that the concentration of the initiator (H0) may be the limiting factor at shorter reaction times.

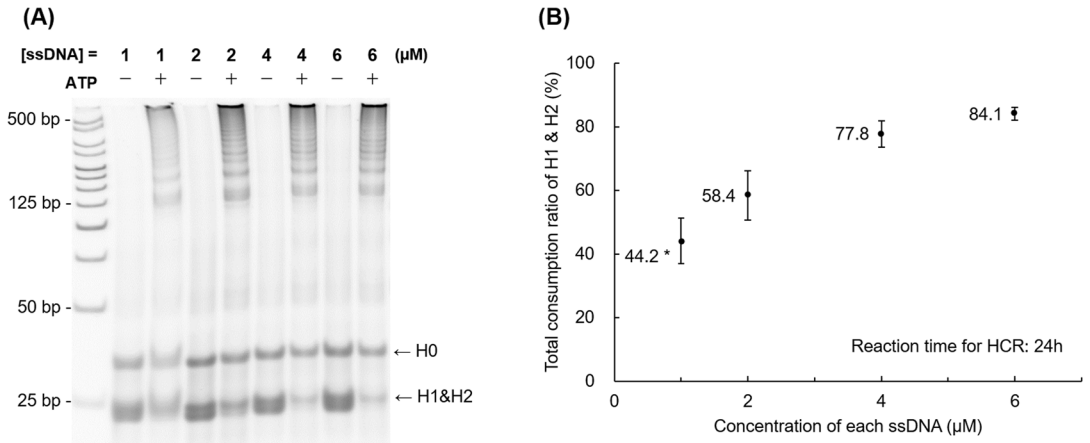

Fig. 2 Effect of total ssDNA concentration on the reaction rate of aptamer-triggered HCR within 24 h. (A) Gel electrophoresis analysis for HCR products after mixing H0, H1, H2 in the presence and absence of ATP with different concentration. (B) The total consumption ratio of H1 and H2 ssDNA in the presence of ATP depending on the ssDNA concentration, quantified from the bands of [H1] and [H2] in (A). Experimental condition: [H0] = [H1] = [H2] = 1–6 μM, [ATP] = 1.4 mM, [$MgCl_2$] = 10 mM, [NaCl] = 300 mM, reaction time for HCR: 24 h. *The 44.2 of consumption ratio was obtained under the same experimental condition reported previously[15] ([H0] = [H1] = [H2] = 1 μM). Data represent mean ± SEM of four independent experiments.

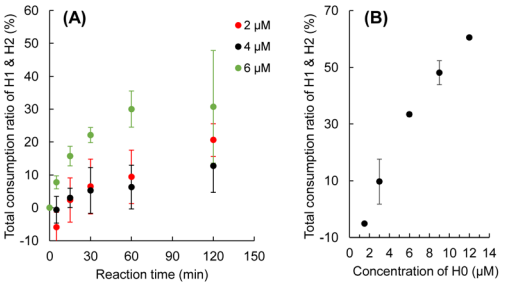

Fig. 3 Effect of the concentration of (A) total ssDNA and (B) H0 on the reaction rate of aptamer-triggered HCR within 2 h. Experimental condition: (A) [H0] = [H1] = [H2] = 2–6 μM; [ATP] = 1.4 mM, [$MgCl_2$] = 10 mM, [NaCl] = 300 mM, reaction time for HCR: 0–120 min. Data represent mean ± SEM of five independent experiments. (B) [H0] = 0–12 μM, [H1] = [H2] = 6 μM, [ATP] = 1.4 mM, [$MgCl_2$] = 10 mM, [NaCl] = 300 mM, reaction time for HCR: 60 min. Data represent mean ± SEM of four independent experiments.

We then specifically investigated the impact of the initiator (H0) concentration while maintaining the hairpin substrate (H1 and H2) concentration high. Fig. 3B shows the total consumption ratio of H1 and H2 when the substrate concentration was fixed at 6 μM, and the H0 concentration was varied from 0 to 12 μM. The results clearly showed that a higher concentration of H0 led to a greater consumption of H1 and H2. Significantly, when the H0 concentration was in the range of 6–9 μM with 6 μM substrate concentration, the consumption ratio reached approximately 40% at 60 minutes. This value is nearly equivalent to the 44.2% consumption ratio achieved under the 24-hour reaction condition, which is asterisked in Fig. 2B ([H0] = [H1] = [H2] = 1 μM). These results clearly indicate that the increased amount of initiator and substrate is highly effective for accelerating the reaction rate of aptamer-triggered HCR, providing a critical step towards realizing rapid detection.

Following the optimization of ssDNA concentrations, we investigated the influence of monovalent salt (NaCl) and divalent salt ($MgCl_2$) concentrations on the HCR reaction rate over a 60-minute incubation period. Appropriate salt concentrations

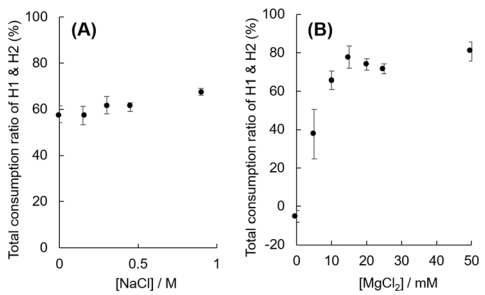

Fig. 4 Effect of the concentration of (A) NaCl and (B) $MgCl_2$ on the reaction rate of aptamer-triggered HCR with 1 h reaction time. Experimental condition: (A) [H0] = 12 μM, [H1] = [H2] = 6 μM, [ATP] = 1.4 mM, [$MgCl_2$] = 10 mM. Data represent mean ± SEM of four independent experiments. (B) [H0] = 12 μM, [H1] = [H2] = 6 μM, [ATP] = 1.4 mM, [NaCl] = 300 mM. Data represent mean ± SEM of three independent experiments.

are crucial for neutralizing the negative charge of the DNA backbone, which stabilizes the resulting double-stranded HCR polymers and facilitates the hybridization process. Fig. 4A shows the effect of varying NaCl concentration on the total consumption ratio of H1 and H2. The results indicate that the concentration of NaCl did not significantly correlate with an increase in the HCR reaction rate over the range tested. Notably, even in the absence of NaCl with 10 mM of $MgCl_2$, the HCR reaction still proceeded efficiently. In contrast, the concentration of $MgCl_2$ was found to be highly critical for driving the HCR reaction. As shown in Fig. 4B, the HCR reaction rate exhibited a strong dependency on the $MgCl_2$ concentration. The consumption ratio of H1 and H2 increased steadily as the $MgCl_2$ concentration was raised from 0 mM up to 10 mM. Above this threshold, specifically in the range of 10–15 mM and beyond (up to 50 mM), the HCR reaction rate plateaued and remained high, suggesting that 10 mM $MgCl_2$ is sufficient to saturate the requirement for stabilizing the DNA structures and promoting hybridization. This clear concentration-dependent trend underscores the essential role of the divalent cation (Mg^{2+}) in facilitating the HCR mechanism, likely by reducing the electrostatic repulsion between the ssDNA strands more effectively than the monovalent Na^+ ions. Furthermore, Mg^{2+} ions are known to be indispensable for the proper folding and function of many DNA aptamers, including the ATP-binding aptamer sequence contained within the H0 strand, which is essential for initiating the ATP-triggered HCR process.

Optimization of mixing condition for HCR products with AuNPs for rapid visual ATP detection

The previous investigations using the experimental results in Fig. 2–4 confirmed that high concentrations of ssDNA (especially the initiator H0) and the presence of at least 10 mM $MgCl_2$ are highly effective for accelerating the aptamer-triggered HCR process. However, it is crucial to recognize a fundamental conflict when integrating these optimized HCR conditions with the AuNP-based colorimetric detection system. Specifically, high ssDNA concentration that promote rapid HCR also enhance the dispersion stability of the AuNPs. This heightened stability can severely prevent the reaction of AuNP aggregation. Conversely, while high concentrations of $MgCl_2$ promote HCR, they also act as potent aggregators for the AuNPs, potentially leading to false-positive aggregation and a diminished signal window. Therefore, the conditions determined to optimize the HCR reaction rate alone are not necessarily the optimal conditions for the final visual detection system. The subsequent step was thus to meticulously optimize the crucial mixing conditions between the HCR product and the AuNP solution to balance the need for both rapid HCR progression and effective colorimetric readout.

To evaluate the performance of the integrated rapid visual detection system, we first examined the colorimetric response using HCR products incubated for 60 minutes and immediately mixed with the AuNP solution (Fig. 5 and S1). The results showed that the method was capable of visually detecting ATP concentrations in the range of 100–500 μM. Furthermore, Fig. 5

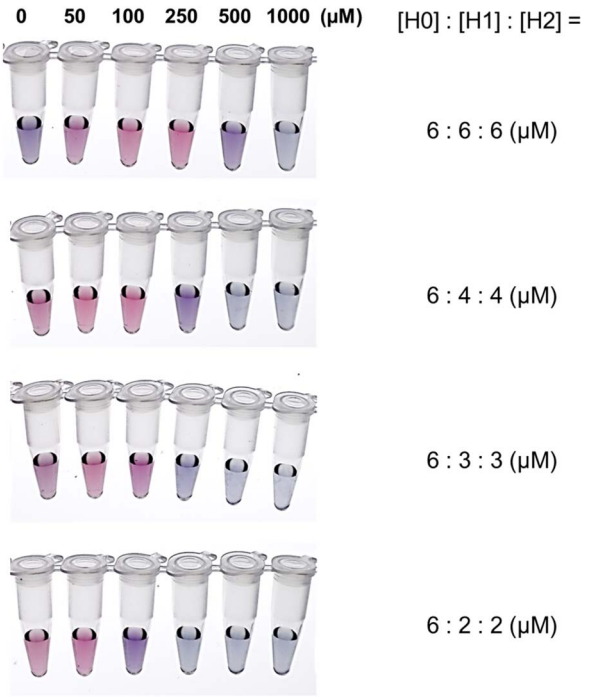

Fig. 5 ATP concentration dependences in the color development of AuNPs at different concentration ratio of H0, H1, and H2 after 10 min HCR incubation time. These color changes were observed 5 min after mixing the HCR product with AuNP solution at 25 °C. Mixing conditions: 60 μL of AuNP solution with 4 μL of HCR solution. HCR was carried out under the experimental condition as follows; $[MgCl_2]$ = 10 mM, [NaCl] = 300 mM. Similar results were obtained in three independent experiments.

highlights the significant impact of the ssDNA concentration ratio on the visual detection sensitivity. Comparing the four conditions—[H0] : [H1] : [H2] = 6 : 6 : 6 μM, 6 : 4 : 4 μM, 6 : 3 : 3 μM and 6 : 2 : 2 μM—the last condition exhibited a lower ATP detection concentration. This difference is strongly attributable to the lower total ssDNA amount in the 6 : 2 : 2 μM condition, which inherently renders the AuNPs less stable and therefore more susceptible to aggregation and color shift upon HCR consumption, effectively improving the visual sensitivity.

We simultaneously focused on reducing the total detection time by investigating shorter HCR incubation times (Fig. 5 and S1). The results revealed that an HCR incubation time of only 10 minutes was sufficient for effective visual detection. Specifically, even at 10 minutes, the assay could clearly distinguish ATP at 100 μM through a visible color difference. Under the [H0] = [H1] = [H2] = 1 μM condition, the HCR barely proceeded within 120 min due to the insufficient substrates' concentrations (data not shown). Therefore, conditions such as 6 : 1 : 1 μM, which involve even lower substrates levels, were not considered in this study. A comparison between the two conditions tested at 20 minutes, [H0] = [H1] = [H2] = 3.2 μM and 4.8 μM, again demonstrated that the condition with the higher total ssDNA concentration (4.8 μM) exhibited greater AuNP dispersion stability, leading to a less pronounced color shift, confirming the trade-off between HCR efficiency and AuNP signal generation (Fig. S2).

A crucial achievement of this optimization is the substantial reduction in the total assay time compared to previous reports. Gao *et al.* (2017) utilized a system requiring an 80-minute HCR incubation at 37 °C followed by an additional 50-minute post-mixing for visual detection, resulting in a total assay time of 130 minutes. In contrast, the colorimetric results shown in this study shown in Fig. 5 demonstrate that with the appropriately optimized mixing ratio between the HCR product and the AuNP solution, immediate visual determination of the ATP concentration is possible at room temperature (25 °C), where the total detection time is approximately 15 minutes, representing a significant reduction compared to the 130 minutes required by Gao and co-workers.

Through the systematic optimization of the total ssDNA concentration, their ratio, cation concentration, and the mixing ratio of HCR product with AuNPs, this study demonstrated the capability for rapid visual detection of ATP at the 100 μM level within 15 minutes. Despite the successful achievement of rapid detection, further improvements in visual detection sensitivity are possible. Potential strategies include the optimization of the volume ratio between the HCR product and the AuNP solution, the use of differently sized AuNPs to tune the stability threshold, and the post-mixing addition of a salt, such as $NaNO_3$, like the method implemented by Gao *et al.*, to further enhance the aggregation kinetics and sharpen the colorimetric response.

Specificity evaluation of the rapid visual ATP detection system

To evaluate the substrate specificity of the developed rapid visual ATP detection system, ATP and its structural analogs nucleoside triphosphates (NTPs), CTP, GTP and UTP were used under the optimized HCR reaction conditions. After HCR reaction, the HCR products were mixed with the AuNP solution for visual detection. As shown in Fig. S3, only the reaction performed in the presence of ATP induced a distinct colorimetric response from red to blue, whereas the other NTP did not produce an appreciable colorimetric response. These results indicated that the established rapid visual detection system exhibited high specificity toward ATP over other NTPs.

Experimental

Materials and reagents

All oligonucleotides used in this study were purchased from Eurofins Genomics (Tokyo, Japan), and purified through oligonucleotide purification cartridge (OPC). The 0.1 M phosphate buffer solution (PBS), and NaCl powder were produced by Fujifilm (Tokyo, Japan). The $MgCl_2 \cdot 6H_2O$ powder was sourced from Fujifilm Wako (VA, USA). The 1 M Tris–HCl buffer (pH 7.5) was obtained from Nippon Gene (Tokyo, Japan). The ATP solution (100 mM) was acquired from Thermo Fisher Scientific (MA, USA). The 15 nm-diameter gold nanoparticles (AuNPs) solution was purchased form Sigma-Aldrich (MO, USA). The commercial acrylamide/bis mixed solution and 1× tris–borate–EDTA (TBE) buffer were purchased from Nacalai Tesque (Kyoto,

Japan), and the GelStar® nucleic acid staining was produced by Lonza (Basel, Switzerland). The nucleoside triphosphates (NTP) bundle (containing ATP, CTP, GTP and UTP 100 mM solutions) was acquired from Thermo Fisher Scientific (MA, USA).

Aptamer-triggered hybridization chain reaction

DNA stock solutions (H0, H2, H1) underwent thermal denaturation at 95 °C for 2 min, then cooled to room temperature. DNA stock solutions diluted to different final concentrations (1, 2, 4 or 6 μM) for HCR reaction, and 4 μL of each were combined sequentially (12 μL total). Then, 4 μL of sample solutions were added sequentially in a total volume of 16 μL. As sample solutions, 4 μL of NTPs (ATP, CTP, GTP and UTP) or NTP free buffer was added. The reaction buffer comprised 1 M Tris–HCl, 0.1 M PBS (pH 7.6), and additional NaCl (0, 0.15, 0.3, 0.45, 0.9 M) and $MgCl_2$ (0, 5, 10, 15, 20, 25, 50 mM) solution with different final concentrations. Reactions incubated at room temperature (25 °C), for 10 minutes to 24 hours.

Native poly acrylamide gel electrophoresis

The 10% native polyacrylamide gels were prepared were prepared using commercial acrylamide/bis mixed solution and 1× TBE buffer. 2 μL samples were loaded onto gels, then ran at 150 V for 35 min in 1× TBE buffer, stained for 15 min in a solution containing 0.01% GelStar® nucleic acid staining, and visualized under UV light. The quantification of the DNA bands was performed using ImageJ software.

Visual detection of ATP samples

The colorimetric assay by naked eye utilizing AuNPs was performed as described below. Briefly, 4 μL of 10–60 minutes HCR samples mixed with 60 μL AuNP solution, then 5 minutes later, visual detection was carried out at room temperature.

Conclusions

In summary, this work successfully established a fast and simple visual detection method for ATP by systematically optimizing the kinetics of the aptamer-triggered HCR and the colorimetric readout process involving AuNPs. We elucidated that the rapid acceleration of HCR is predominantly achieved through the optimization of ssDNA concentrations and the essential role of Mg^{2+}, which significantly contributes to both DNA hybridization and aptamer folding. Recognizing the conflicting requirements for fast HCR and stable AuNP dispersion, we then fine-tuned the mixing conditions between the HCR product and the AuNP solution. This integrated optimization resulted in a high-performance system capable of visually detecting ATP at the 100 μM level with a total assay time of approximately 15 minutes, marking a substantial reduction in analysis time compared to existing AuNP-based HCR methods. While the current detection level serves as an excellent proof-of-concept for rapid analysis, the sensitivity can be further enhanced by incorporating strategies such as optimizing the AuNP particle size, adjusting the sample-to-AuNP mixing ratio, and introducing post-mixing salt treatments like $NaNO_3$ for improved aggregation kinetics. The threshold for ATP concentration changes from red to blue can be easily controlled by adjusting the mixing ratio of gold nanoparticles and single-stranded DNA. This characteristic enables threshold-based visual detection, specifically clear binary (positive/negative) visual detection at the target ATP concentration. Therefore, we believe this method offers practical value for biological contamination screening in industrial and environmental fields rather than clinical diagnosis, enabling more robust applications than clinical diagnostics.

Author contributions

The study was jointly conceived and designed by all authors. S. Z. and K. Y. were responsible for the initial drafting of the manuscript. S. Z., H. F., S. W. and W. L. participated in the material preparation, data collection, and analysis. All authors critically reviewed and provided feedback on previous versions of the manuscript. S. Z., M. Y., M. M., K. O., Y. Y. and K. Y. made contributions to revising and finalizing the manuscript. All authors read and approved the final manuscript.

Conflicts of interest

The authors declare no competing interests.

Data availability

Data will be prepared available upon request.

Supplementary information (SI) is available. See DOI: https://doi.org/10.1039/d5ay01738f.

Acknowledgements

This research was supported by the joint research program between the University of Tokyo and Daikin Industries, Ltd based on university-corporate relations agreement.

Notes and references

1 F. Pistelok, A. Pohl, T. Stuczyński and B. Wiera, *Ecol. Chem. Eng. S*, 2016, **23**, 259–270.
2 P. Connolly, S. F. Bloomfield and S. P. Denyer, *J. Appl. Bacteriol.*, 1993, **75**, 456–462.
3 M. Bakke, *J. Food Prot.*, 2022, **85**, 1079–1095.
4 J. H. Sogin, G. L. Velasco, B. Yordem, C. K. Lingle, J. M. David, M. Cobo and R. W. Worobo, *Appl. Environ. Microbiol.*, 2021, **87**, e02278.
5 Y. Zhang, Y. Wu, A. Guo, Y. Liu, Q. Sun, X. Zou and Z. Sun, *Anal. Methods*, 2025, **41**, 8298–8316.
6 G. Shama and D. J. Malik, *Int. J. Hyg. Environ. Health*, 2013, **216**, 115–125.
7 N. Omidbakhsh, F. Ahmadpour and N. Kenny, *PLoS One*, 2014, **9**, e99951.
8 G. S. Whiteley, C. Derry, T. Glasbey and P. Fahey, *Infect. Control Hosp. Epidemiol.*, 2015, **36**, 658–663.
9 J. Liu and Y. Lu, *J. Am. Chem. Soc.*, 2007, **129**, 8634–8643.

10 F. Li, J. Zhang, X. Cao, L. Wang, D. Li, S. Song, B. Ye and C. Fan, *Analyst*, 2009, **134**, 1355–1360.
11 K. M. Song, M. Cho, H. Jo, K. Min, S. H. Jeon, T. Kim, M. S. Han, J. K. Ku and C. Ban, *Anal. Biochem.*, 2011, **415**, 175–181.
12 Y. F. Tian, W. Zhou, B. C. Yin and B. C. Ye, *Anal. Methods*, 2017, **9**, 6038–6043.
13 S. Zhang, K. Wang, J. Li, Z. Li and T. Sun, *RSC Adv.*, 2015, **5**, 75746–75752.
14 C. Yang, Y. Wang, J.-L. Marty and X. Yang, *Biosens. Bioelectron.*, 2011, **26**, 2724–2727.
15 Y. Tu, J. Wu, K. Chai, X. Hu, Y. Hu, S. Shi and T. Yao, *Talanta*, 2023, **260**, 124649.
16 Y. Zhu, P. Chandra and Y.-B. Shim, *Anal. Chem.*, 2013, **85**, 1058–1064.
17 R. M. Dirks and N. A. Pierce, *Proc. Natl. Acad. Sci. U. S. A.*, 2004, **101**, 15275–15278.
18 C. Zhang, J. Chen, R. Sun, Z. Huang, Z. Luo, C. Zhou, M. Wu, Y. Duan and Y. Li, *ACS Sens.*, 2020, **5**, 2977–3000.
19 H. M. T. Choi, V. A. Beck and N. A. Pierce, *ACS Nano*, 2014, **8**, 4284–4294.
20 Q. Wang, X. Yang, X. Yang, K. Wang, H. Zhang and P. Liu, *Analyst*, 2015, **140**, 7657–7662.
21 R. Li, L. Zou, Y. Luo, M. Zhang and L. Ling, *Sci. Rep.*, 2017, **7**, 44212.
22 J. Chen, J. Tang, H. M. Meng, Z. Liu, L. Wang, X. Geng, Y. Wu, L. Qu and Z. Li, *Chem. Commun.*, 2020, **56**, 9024–9027.
23 C. Li, L. Guo, X. Sang, X. Jiang, H. Wang, P. Qin and L. Huang, *Talanta*, 2023, **258**, 124453.
24 A. Khan, H. Khan, N. He, Z. Li, H. K. Alyahya and Y. A. B. Jardan, *Front. Immunol.*, 2025, **15**, 1479403.
25 Z. Gao, Z. Qiu, M. Lu, J. Shu and D. Tang, *Biosens. Bioelectron.*, 2017, **89**, 1006–1012.
26 D. E. Huizenga and J. W. Szostak, *Biochemistry*, 1995, **34**, 656–665.